

Effects of Time-Varying Basic-State Flow by Cloud Momentum Flux on Multicell-Type Storms

Hye-Yeong Chun¹, In-Sun Song¹ and Jong-Jin Baik²

¹Department of Atmospheric Sciences and Global Environment Laboratory Yonsei University

²School of Earth and Environmental Sciences Seoul National University

(Manuscript received 1 December 2001; accepted 20 December 2001)

ABSTRACT

Effects of time-varying basic-state flow by the cloud momentum flux on multicell-type convective system are investigated using a two-dimensional cloud model. Two numerical experiments are performed, the control simulation with constant basic-state wind and the variable simulation with time-varying basic-state wind. The amount of change in the basic-state wind in the variable simulation is calculated by the vertical convergence of the momentum flux induced by clouds. It is shown that the change in the basic-state wind by the cloud momentum flux is as large as $10 \text{ m s}^{-1}/\text{hr}$. Especially, the cloud momentum flux in the troposphere increases positive shear in the lower troposphere and produces negative shear in the mid-troposphere and positive shear in the upper troposphere. This results in a significant structural change of the mesoscale convective system. The control simulation exhibits typical characteristics of multicell-type convective storms, that is, a new convective cell is periodically produced behind the gust front updraft. However, in the variable simulation, convection is concentrated in the gust front updraft region and the periodic regeneration of convective cell behind the gust front updraft disappears. This is because very weak storm-relative mid-level inflow prevents a separation of convective cell from the gust front updraft, which is essential for the cell regeneration in multicell-type convective storms.

Key words: multicell-type convective storms, basic-state wind, cloud momentum flux

1. Introduction

The importance of environmental wind structure on mesoscale convective system has long been recognized by observations (Newton 1950; Newton and Newton 1959; Ogura and Liou 1980). Many theoretical (Moncrieff and Green 1972; Thorpe *et al.*, 1980) and numerical modeling studies (Weisman and Klemp 1982; Rotunno *et al.*, 1988; Weisman *et al.*, 1988; Lafore and Moncrieff 1989; Fovell and Dailey 1995) have revealed that environmental wind shear is a major factor in characterizing storm structure for a given atmospheric stability condition.

An investigation of the role of environmental wind shear and rain-produced cold pool on the maintenance of long-lived convective system has been one of main

research topics in mesoscale numerical modeling studies. Weisman and Klemp (1982) showed that mesoscale convective storms can be characterized based on the bulk Richardson number which is a ratio between the convective available potential energy and environmental wind shear. Thorpe *et al.* (1982) proposed that a strong low-level wind shear can prevent outflow from moving away from convective system and it can be a favorable condition for long-lived convective system. Rotunno *et al.* (1988) suggested that when the cold pool is balanced by the wind shear, the circulation induced by the cold pool trying to spread downshear is opposed by the wind shear and deep penetration may take place. They also suggested an optimal structure of environmental wind for long-lived convective system, which has strong positive shear from the surface to a height of 2.5 km and constant wind above. Fovell and Dailey (1995) investigated multicell-type storm dynamics from the view of cell generation and oscillation periodicity according to the environmental wind structure.

In the numerical modeling studies of convective storms including the above-mentioned studies, environmental

Corresponding Author: Hye-Yeong Chun, Department of Atmospheric Sciences, Yonsei University, Seoul 120-749, Korea

Phone : +82-2-2123-2692

E-mail : chy@atmos.yonsei.ac.kr

wind is assumed to remain fixed with time throughout model integration. This may be based on the assumption that environmental wind, which is large-scale flow, is not changed much by convective clouds during a time scale of several hours. That is, only one-way interaction from the large-scale flow to mesoscale convective system is considered. However, organized mesoscale convective system can significantly modify environmental wind structure by thermal and mechanical forcing even with a time scale of several hours. Using the observational data during the GATE (GARP Atlantic Tropical Experiment), LeMone (1983) showed that the momentum flux normal to the line of cumulonimbus is associated primarily with the westward acceleration of an upward-moving buoyant convective core by mesoscale pressure gradient force and that the horizontally averaged momentum flux can accelerate/decelerate environmental wind as much as $2 \text{ m s}^{-1}/\text{hr}$. It was shown that the momentum flux increases U -shear in the tropical squall-line case. For the mid-latitude squall lines simulated using a cloud model, Fovell *et al.* (1992) showed that the maximum basic-state wind acceleration in the lower troposphere associated with the cloud momentum flux is about $2 \text{ m s}^{-1}/\text{hr}$. The basic-state wind increases in the lower troposphere and decreases in the mid- to upper troposphere. Accordingly, wind shear increases by the cloud momentum flux.

It is noteworthy that feedback between the large-scale basic-state flow and mesoscale perturbations cannot be automatically considered by simply running a nonlinear mesoscale numerical model in a two-dimensional, non-rotating framework. This is because timely or/and horizontally averaged model-produced wind in a non-rotating framework is not the basic-state wind representing the large-scale flow in thermal wind balance. Mesoscale convective storms can only modify the large-scale flow through the convergence/divergence of convective momentum flux. In order for the model-produced horizontally-averaged wind at any time to be a large-scale flow in a two-dimensional, non-rotating framework, external forcing has to be included as done by Hauf and Clark (1989).

In large-scale models, convective clouds are considered as a main subgrid-scale thermal forcing and, in some aspects, a two-way interaction between the large-scale flow and convective clouds is allowed through cumulus

parameterization. Interaction between cumulus ensembles and large-scale flow has been extensively studied using numerical cloud models (Soong and Tao 1980; Dudhia and Moncrieff 1987; Tao *et al.*, 1987; Krueger 1988) and model results have been used for validation of cumulus parameterization. Recently, Moncrieff (1992) theoretically examined the dynamical effects of organized convective system on the large-scale flow. He showed that the momentum flux by organized convective system increases the basic-state wind shear normal to the convective line. This result is different from that based on the traditional mixing length theory. Wu and Moncrieff (1996) proposed a way to parameterize the effects of the momentum flux by organized convective system for large-scale models.

In most of the numerical modeling studies of mesoscale convective system, the influence of time-independent large-scale flow on storm development and maintenance has been investigated and the effects of the momentum flux by organized convective system developed under time-independent large-scale flow have been parameterized in large-scale models. In some senses, a scale interaction between the large-scale flow and mesoscale convective system imbedded in it has not been considered. However, for organized mesoscale convective system with a time scale of more than six hours, variability of the basic-state wind by the cloud momentum flux might not be negligible. Thus, it is better to consider the development of organized convective system under time-varying basic-state flow by convection itself in 2-dimensional, non-rotating model framework.

In this study, we will numerically investigate interaction between large-scale flow and multicell-type convective system by allowing for time-varying basic-state wind associated with the vertical convergence/divergence of cloud momentum flux. In section 2, a brief description of the numerical model used in this study and a methodology to include time-varying basic-state wind forcing to mesoscale numerical model are given. In section 3, results from the simulated multicell-type convective system in a time-independent basic-state wind are presented and the momentum flux and its associated variability of the basic-state wind are discussed. In section 4, results from the simulated convective system in time-dependent basic-state flow are presented. Effects of time-varying basic-state wind

on the development and maintenance of multicell-type storms are discussed with an emphasis on cell generation and periodicity. Finally, summary and conclusions are given in section 5.

2. Numerical Model

The numerical model used in this study is the ARPS (Advanced Regional Prediction System) developed at the CAPS (Center for Analysis and Prediction of Storms) of the University of Oklahoma (Xue *et al.*, 1995). The ARPS is a three-dimensional, nonhydrostatic, compressible, cloud-resolving model with explicit liquid and ice phase cloud microphysical processes. A detailed description of the model can be found in the ARPS User's Guide (Xue *et al.*, 1995).

In this study, we employ a two-dimensional version of the model. For the subgrid-scale mixing processes, Smagorinsky (1963) turbulence scheme is used. The ice phase cloud processes and surface processes are excluded and the rotational effect of the Earth is neglected. All the simulations are performed on a model domain of 1500 km wide and 36 km deep. The grid spacing is 1 km in the horizontal and 300 m in the vertical. A two-time-step process is employed with a large time step of 3 s and a small time step of 1 s in order to take care of sound waves for compressible flow. A wide horizontal computational domain is chosen because of the poor behavior of lateral boundary conditions. Neither the radiation boundary condition originally proposed by Orlanski (1976) nor that by Klemp and Wilhelmson (1978) with specified constant phase speeds in a range of $c^* = 30\text{--}40 \text{ m s}^{-1}$ satisfied proper wave propagation at the upstream edge of the boundary in this highly nonlinear flow simulation. Besides the nonlinearity, the lateral boundary condition is especially important in this study because the variable basic-state wind forces to change the total wind at each time step at the lateral boundaries. In order to overcome these problems, we included a sponge layer near the inflow boundary (right boundary) in which the dissipation (Rayleigh damping and Newtonian cooling) is gradually enhanced to a maximum at the boundary. At the outflow boundary (left boundary), a modified Orlanski's radiation condition with vertically averaged phase speed, named

the Klemp, Lilly, and Durran radiation scheme in the ARPS, is used. A sponge layer with the Rayleigh damping and Newtonian cooling is located in a layer of the uppermost 9 km to suppress artificial reflection of gravity waves from the upper boundary.

In the simulations herein, the thermodynamic structure of the basic-state flow is specified according to the analytic sounding of Weisman and Klemp (1982). This thermodynamic sounding possesses a convective available potential energy (CAPE) of 2489 J kg^{-1} for an air parcel lifted from the surface. Lifting condensation level is located at $z = 1.1 \text{ km}$ and the level of free convection is at $z = 1.6 \text{ km}$. A lifted parcel from the surface becomes neutrally buoyant at $z = 11.4 \text{ km}$. There exists a convective inhibition of -54 J kg^{-1} at low layer. Characteristics of this sounding are similar to those in severe mid-latitude squall lines and it is widely used for two-dimensional, long-lived squall-line simulation. Above the tropopause at $z = 12 \text{ km}$, the model atmosphere is stably stratified with a Brunt-Vaisala frequency of about 0.02 s^{-1} , representing the stratosphere. The initial basic-state wind is assumed to increase linearly from the surface to $z = 6 \text{ km}$ and remain constant above. In order to keep convective and stratiform features of simulated storm in the central portion of the model domain after its organization, the Galilean transform (18 m s^{-1}) is applied to the basic-state wind profile (Fig. 1). Convection is initiated using a 2 K ellipsoidal warm bubble that has a horizontal radius of 5 km and a vertical radius of 1.5 km and is centered at $x = 800 \text{ km}$ and $z = 1.5 \text{ km}$.

In this study, two types of numerical simulations are performed, the control simulation with the time-independent basic-state wind shown in Fig. 1 and the simulation, named the variable simulation, with time-dependent basic-state wind associated with the cloud momentum flux. The experimental design of the variable simulation is described in section 4. For both the control and variable simulations, numerical integration is carried out for 12 hours.

3. Control Simulation

Simulated storm represents a typical multicell-type storm that is characterized by periodic cell generation,

development, and decay processes. Note that the computed bulk Richardson number using the basic-state wind and CAPE used in this study is 12.45. This value is marginally in the regime of multicell-type storms based on the numerical experiments by Weisman and

Klemp (1982).

Figure 2 shows the time series of the domain maximum vertical velocity in the control simulation. The convective system persists throughout the simulation of 12 hours. During the development stage (before $t = 4\text{ h}$), the maximum vertical velocity increases up to 25 m s^{-1} at $t = 170 \text{ min}$ with somewhat irregular oscillations. During the mature stage (after $t = 4 \text{ h}$), the maximum vertical velocity reduces to values of less than 16 m s^{-1} with irregular oscillations before $t = 550 \text{ min}$ and regular oscillations after that. A spectral analysis of the time series of the domain maximum vertical velocity at the mature stage (not shown) revealed that a primary oscillation period is about 18.3 min. At the development stage, the maximum vertical velocity tends to increase with time by enhancing the strength of the cold pool or gust front. Once the negative vorticity induced by the cold pool dominates the positive vorticity by the basic-state wind, the updraft tilts upshear and the maximum vertical velocity decreases to be quasi-steady.

The evolution of the surface precipitation rate during the mature stage is shown in Fig. 3. The maximum precipitation is observed at about 8 km behind the gust front. The surface precipitation extends about 50 km from the gust front due to the rearward propagation of consecutive convective cells.

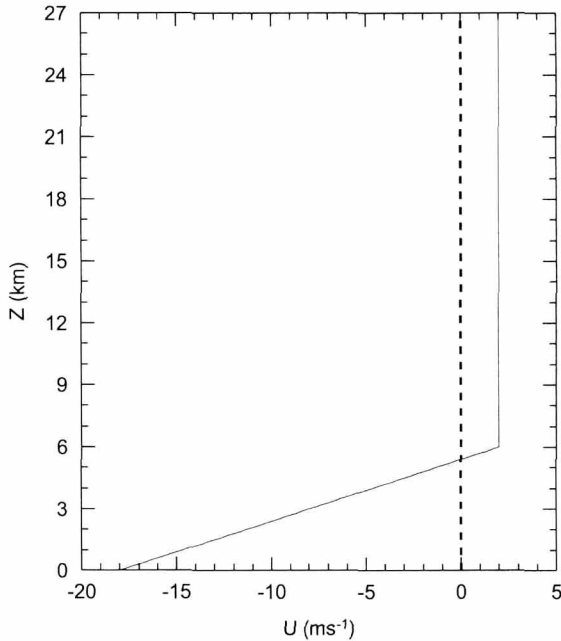


Fig. 1. The basic-state wind structure used in the control simulation.

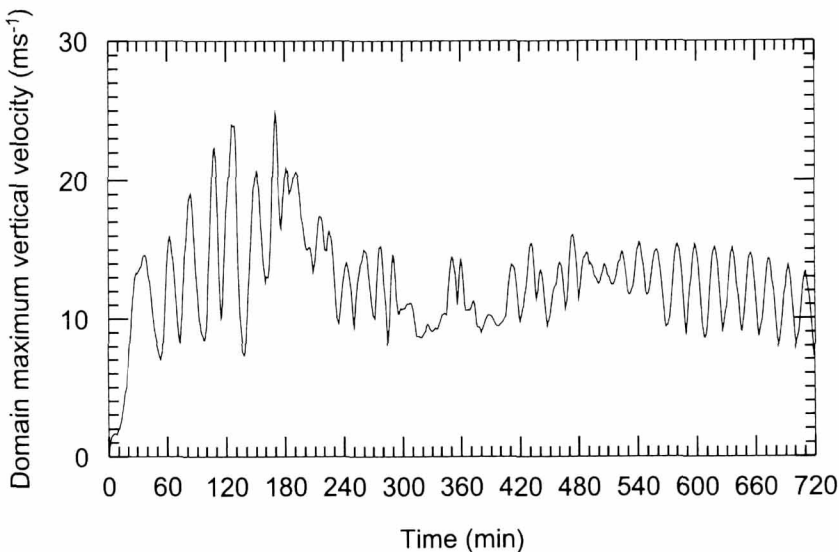


Fig. 2. The time series of the domain maximum vertical velocity in the control simulation.

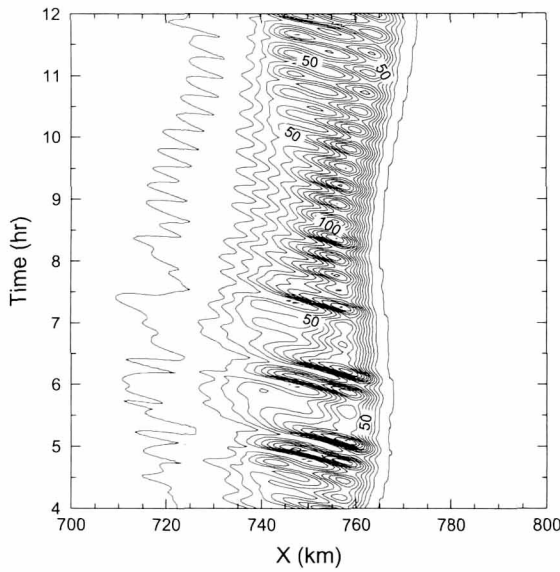


Fig. 3. The evolution of the surface precipitation rate after $t = 4$ h in the control simulation. The contour interval is 10 mm hr^{-1} except that the contours in the left and right boundaries are 0.1 mm hr^{-1} .

Figure 4 shows the evolution of the vertical velocity field superimposed on the perturbation potential temperature field in every 5 min from $t = 9$ h to $t = 9$ h 35 min. This figure clearly shows the periodic behavior of convective cell generation, development, and decay. Because the period of the cell generation is ~ 19 min in the control simulation, the total time sequence in Fig. 4 corresponds to approximately 2 cycles of cell generation. At $t = 9$ h, there exists three convective updrafts cells in the region of $x > 730$ km and several consecutive weak cells behind cell 1. The updraft near $x = 766$ km (denoted by G) is the gust front updraft (GFU) at the head of density current. The updraft centered near $x = 750$ km and $z = 6.5$ km (cell 2) is a major convective cell that produces heaviest surface rainfall (Fig. 3). The cell behind the major cell (cell 1) weakens as it propagates rearward relative to the gust front. This cell was a major convective cell at a time of the previous cycle of cell generation. The downdraft located at the right of the major convective cell is a compensating downdraft. The updrafts and downdrafts tilted upshear above $z = 15$ km are convectively generated internal gravity waves. As shown in Fig. 3, most of the surface precipitation is produced

by the major convective cell and the GFU. At $t = 9$ h 5 min (Fig. 4b), a new cell starts to develop in the region of $750 \text{ km} < x < 760 \text{ km}$, shows up as a cell (cell 3) at $t = 9$ h 15 min (Fig. 4d), and becomes a major cell at $t = 9$ h 20 min (Fig. 4e). The new major convective cell has its maximum strength during the time d-f. This process is repeated again in the next cycle (Figs. 4e-4h).

The periodic regeneration of convective cell has been one of main research topics in numerical modeling studies of multicell-type storms. So far, three mechanisms have been proposed to explain the regeneration of convective cell in multicell storms: 1) a gravity-wave mechanism by Yang and Houze (1995), 2) a cut-off process by internal circulation by Fovell and Tan (1998), and 3) an advection mechanism by Lin *et al.* (1998). In fact, these three mechanisms attempt to explain one essential process for the multiplication of convective cell in different viewpoints. That is a separation of convective cell from GFU, so-called a cut-off process. Using the phase relationship between the simulated variables based on a linear, monochromatic gravity-wave theory, Yang and Houze (1995) suggested that the consecutive cells behind GFU are internal gravity waves trapped in the convective region. They showed that the periodicity of cell regeneration is associated with the phase speed of internal gravity waves. Based on a vorticity argument, Fovell and Tan (1998) suggested that the circulation induced by convective cell itself causes a separation of convective cell from GFU. Lin *et al.* (1998) suggested that the convective cell is advected rearward by the storm-relative mid-level inflow rather than the cut-off from GFU. They showed that the period of cell regeneration is inversely proportional to the magnitude of the storm-relative mid-level inflow. Both Fovell and Tan (1998) and Lin *et al.* (1998) suggested that the growing cell at the early stage and the propagating cell at the later stage of development should be considered differently and showed that only the propagating cell has characteristics of gravity waves.

Analysis of the phase relationship between the perturbation vertical velocity and perturbation potential temperature in the present study revealed (not shown) that only the propagating convective cells have gravity-wave characteristics as mentioned in Yang and

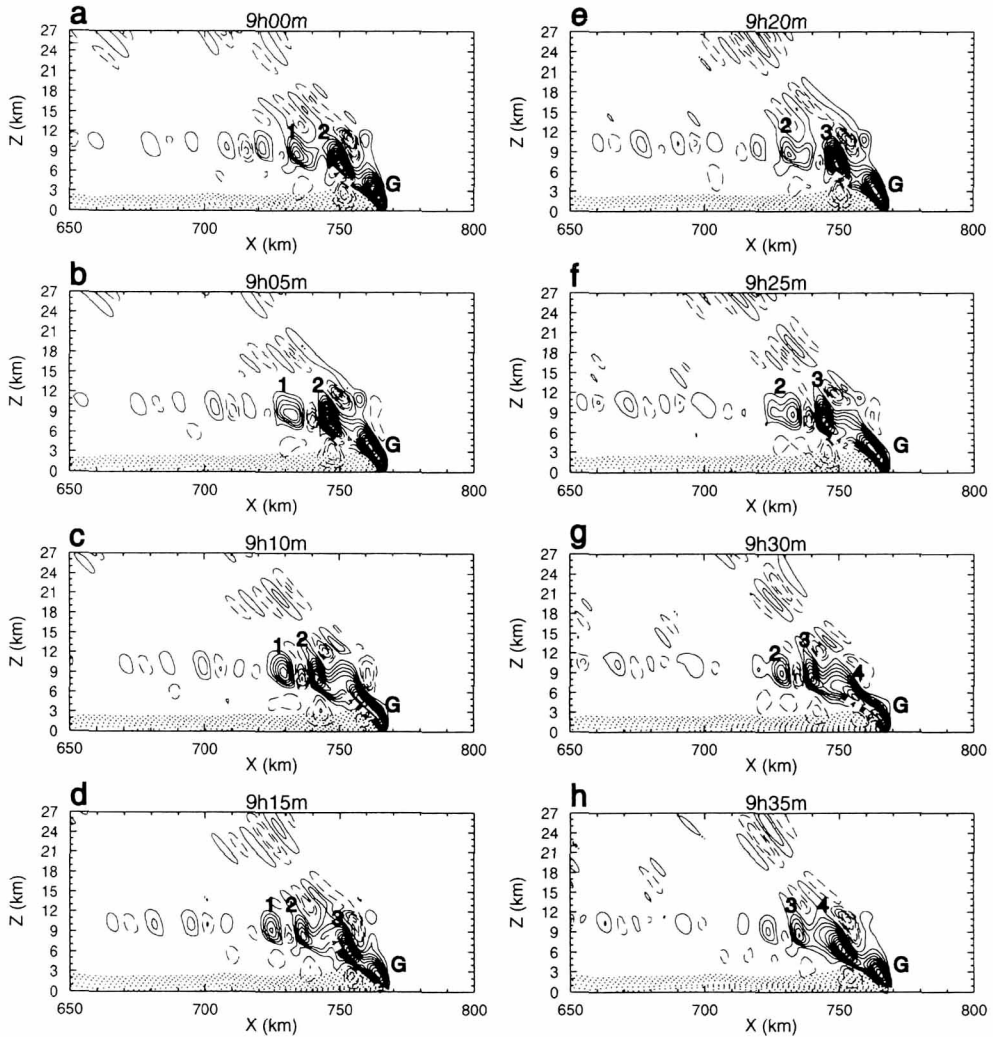


Fig. 4. The evolution of the vertical velocity field superimposed on the perturbation potential temperature field in every 5 min from $t = 9$ h to $t = 9$ h 35 min in the control simulation. Only the negative perturbation potential temperature is plotted to clearly represent the cold outflow. The contour intervals of the vertical velocity and perturbation potential temperature are 1 m s^{-1} and 1 K , respectively

Houze (1995), while the growing convective cells may experience a critical-level amplification under the in-phase relationship between the diabatic heating and vertical velocity as mentioned in Lin *et al.* (1998). It is, however, worth mentioning that the phase relationship between the simulated flow fields, which is often used to check whether the consecutive convective cells are internal gravity waves or not, should be used qualitatively because the situation in the nonlinear, moist convection is much different from that in the linear, dry, monochromatic gravity waves.

The horizontal distribution of the momentum flux at $t = 10$ h at selected heights is shown in Fig. 5. Two interesting features are observed in this figure. First, the momentum flux is concentrated in the region of major updraft ($x = 750 \text{ km}$) with a horizontal scale of less than 20 km. This indicates that the momentum flux is in the convective scale of on the order of 10 km rather than in the mesoscale of 100 km. This is consistent with the aircraft observation analysis of the momentum flux in a tropical squall-line case by LeMone (1983). Secondly, the magnitude and sign of the

momentum flux vary significantly with height. Near the surface, the momentum flux is positive mainly due to a product of the positive perturbation horizontal velocity and the updraft at the gust front. In the cloud region, the magnitude of the momentum flux increases with height up to 6 km and decreases above. Above the cloud region, small negative momentum flux is observed, representing convectively induced internal gravity waves. Note that the scale of the momentum flux at $z = 15$ km is different from that at other heights.

In the present simulation, the cloud-top height is approximately located at $z = 15$ km in the quasi-steady state.

Figure 6 shows the vertical profiles of the horizontally averaged momentum flux ($M = \rho_0 \bar{u} \bar{w}$, where ρ_0 is the basic-state density and \bar{u} and \bar{w} are the perturbation horizontal and vertical velocities, respectively) averaged over each hour of the simulation. The horizontal average is taken over 350 km from $x = 500$ km to 850 km where main convection is occupied.

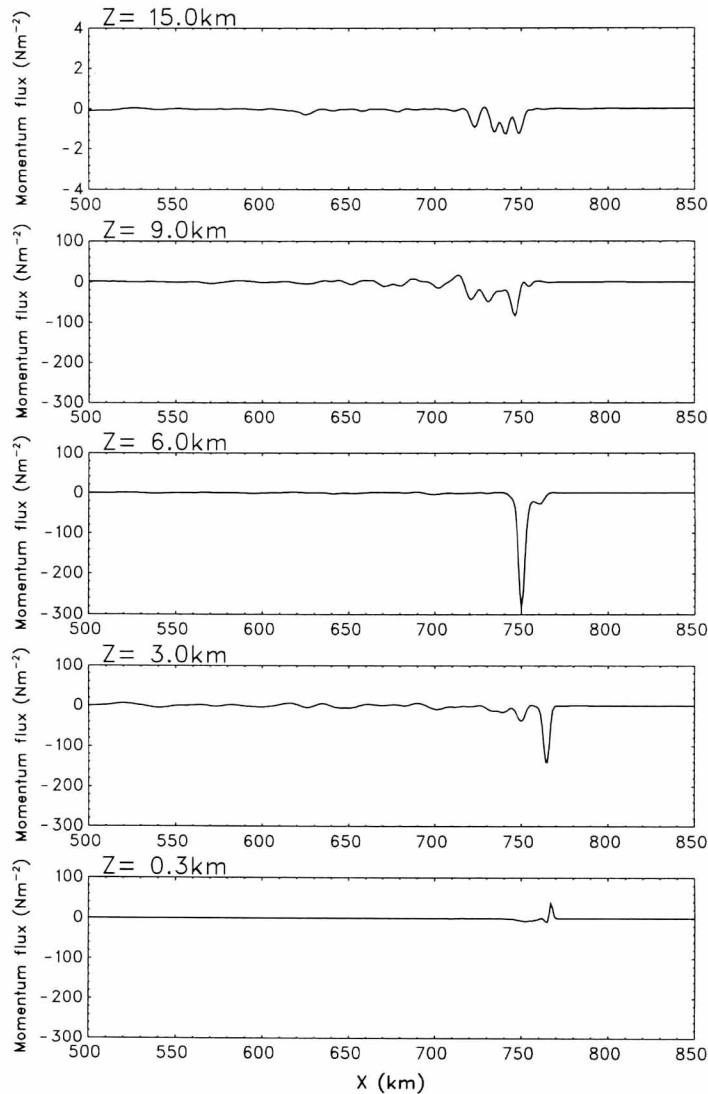


Fig. 5. The horizontal distribution of the momentum flux at $t = 10$ h at selected heights in the control simulation. Note that the scale of the momentum flux at $z = 15$ km is different from that at other heights.

At the early stage of storm development, the momentum flux is positive in the region of $z = 6\text{-}10 \text{ km}$ mainly due to the downshear tilt of updrafts. The magnitude of the momentum flux increases rapidly after $t = 3 \text{ h}$, reaches its maximum at $t = 8\text{-}9 \text{ h}$, and then slightly decreases with time. After 3-4 hours, the negative momentum flux is dominant throughout the convective region with a minimum value of 5.8 N m^{-2} near $z = 6 \text{ km}$ at $t = 8\text{-}9 \text{ h}$. The basic structure of the momentum flux profile after 3 h is similar to that obtained analytically by Moncrieff (1992) (Fig. 6 in his paper), which represents the effects of circulation with a downdraft, and overturning updraft and a jump updraft.

The small negative momentum flux above clouds ($z > 15 \text{ km}$) represents convectively generated internal gravity waves. Even though the magnitude of the momentum flux at the cloud top is much smaller than that in the cloud region, it can play an important role in the basic-state flow in the stratosphere as a

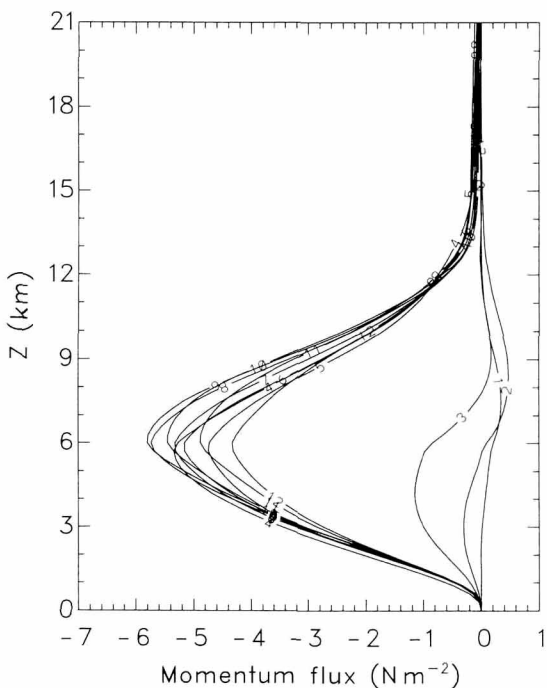


Fig. 6. The vertical profiles of the horizontally averaged momentum flux averaged over each hour of the control simulation. The horizontal average is taken over 350 km from $x = 500 \text{ km}$ to 850 km . The numeric numbers in the figure implies that the profile in the number 3, for example, is time-averaged from $t = 2 \text{ h}$ to 3 h .

gravity-wave drag. If we assume that gravity waves with a momentum flux of -0.1 N m^{-2} at the cloud top are broken at $z = 25 \text{ km}$ by a linear decrease of the momentum flux, the basic-state wind deceleration can be as large as $10 \text{ m s}^{-1}/\text{day}$. This amount of deceleration in the basic-state wind is comparable to that by the mountain drag.

It is important to note that the magnitude of the momentum flux increases rapidly as the convective system approaches its mature stage. This is because the perturbation horizontal velocity is large after $t = 3 \text{ h}$ in the major updraft region even though the magnitude of the vertical velocity is smaller than that at the early stage. Once the convective system reaches its mature stage producing strong negative perturbation horizontal velocity in the front-to-rear inflow region, a negative correlation between the perturbation horizontal velocity and vertical velocity is prominent in the region of major updrafts. The magnitude of the momentum flux in the present study is much larger than that in the observed tropical squall-line case by LeMone (1983) due to the stronger perturbation velocities. Unlike her case, dynamic pressure perturbation is shown to be important in this case, which is a major source for producing upward motion in the convective region.

The cloud momentum flux can change the large-scale flow as a subgrid-scale momentum source or sink. The role of the momentum flux in the large-scale flow can be expressed as:

$$\frac{\partial U}{\partial t} = -\frac{1}{\rho_0} \frac{\partial M}{\partial z}. \quad (1)$$

Here, U is the basic-state wind and M the momentum flux. It is noteworthy that the basic-state wind represents the large-scale environmental flow in which mesoscale convective system is embedded. The temporally and horizontally averaged fields in a two-dimensional, non-rotating numerical model considered in this study do not correspond to an environmental flow because there can be no true split into environment and convection in such a system. The environmental flow can be the slow-manifold, rotationally-constrained flow. The mesoscale convective system in a two-dimensional, non-rotating framework only can modify the environmental flow largely due to the change in the potential vorticity

field brought about by convective mass transport, latent heating/cooling, and mixing. The influence of mesoscale convective system on the large-scale flow can be estimated by calculating the flux divergences of heat, momentum, and moisture, though a portion of the flux divergence is used for generating gravity waves rather than balancing large-scale flow.

Figure 7 shows the vertical profiles of basic-state wind acceleration calculated using (1) and the momentum-flux profiles in Fig. 6. After 3 hours, there exists acceleration with a maximum value of $\sim 6 \text{ m s}^{-1}/\text{hr}$ below $z = 6 \text{ km}$ and deceleration with a minimum value of $\sim -10 \text{ m s}^{-1}/\text{hr}$ above it. Consequently, the momentum flux increases the basic-state wind shear in the lower troposphere (0-5 km) where initially positive shear exists, and produces negative shear in the mid-troposphere (5-9 km) and positive wind shear in the upper troposphere (9-15 km). The magnitude of the acceleration/deceleration of the basic-state wind by the cloud momentum flux is quite significant. As will be presented in the next section, this results in a significant structural change of the storm. The structure of the basic-state wind acceleration/deceleration after

3 hr resembles like the profile obtained analytically by Moncrieff (1992) (Fig. 5 in his paper) for the case with both overturning updraft and downdraft. Note that Fig. 5 in Moncrieff (1992) is the momentum flux divergence, while Fig. 7 in this study is proportional to the momentum flux convergence.

Even though (1) represents a change in the basic-state wind directly by the momentum forcing, the acceleration of the large-scale flow under a thermal wind balance is determined by not only the momentum forcing itself but also the Coriolis acceleration induced by the secondary circulation. The Coriolis acceleration usually compensates for the basic-state wind tendency by the momentum forcing. Therefore, the magnitude of the basic-state wind acceleration can be smaller than that estimated by the momentum forcing only. LeMone (1983) calculated the Coriolis acceleration using observed meridional wind data and showed that the Coriolis acceleration significantly compensates for the basic-state wind tendency. In the present two-dimensional, nonrotational flow case, the Coriolis acceleration cannot be calculated using a meridional wind component. Rather, it may be estimated the Coriolis acceleration of the basic-state wind by considering the linear response of the large-scale flow to the subgrid-scale momentum flux as was done by Palmer *et al.* (1986) in the mountain case. This issue will be briefly discussed in the last section.

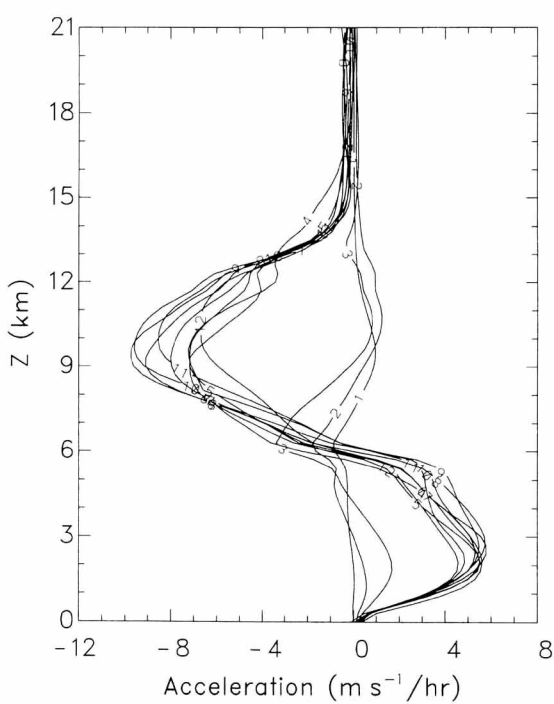


Fig. 7. The acceleration of the basic-state wind by the vertical convergence of the momentum flux in Fig. 6.

4. Variable Simulation

In the variable simulation, the basic-state wind is allowed to change with time by the cloud momentum flux in the atmospheric layer occupied by clouds and the cloud-induced gravity-wave momentum flux above clouds. In the variable simulation, following methodology is applied. The initial basic-state wind is assumed to be constant with time over certain period starting from the beginning of the model integration (phase I) and then is forced to change with time smoothly from the initial structure to the final one for a transition period (phase II). The amount of change in the basic-state wind is calculated using the momentum flux of the simulated convective storm averaged over certain hours during the phase I. The changed basic-state wind remains

constant with time after the phase II period until the end of the simulation (phase III). This procedure is similar to that in Nance and Durran (1997) in the nonstationary lee-wave problem except that they used two idealized basic-state flows (mainly focused on the change in the basic-state thermodynamic structure), while here a basic-state wind calculated using the storm-produced momentum flux was used.

In the variable simulation, the periods of phase I, phase II, and phase III are chosen to be 0-6 h, 6-8 h, and 8-12 h, respectively. A reason for choosing the period of phase I as 6 hours is that the multicell storm reaches mature stage after 4 hours and 2 h-averaged momentum flux is needed at the mature stage. There is no specific physical reason to choose the transition period of 2 hours. The 2 h-averaged change in the basic-state wind, which is horizontally uniform, is evenly added to the total horizontal velocity at every time step from $t = 6$ h to 8 h. Because the ARPS model predicts the total horizontal velocity, a change in the basic-state wind is felt through a change in the total horizontal velocity.

Figure 8 shows the modified basic-state wind profile together with the initial basic-state wind profile shown in Fig. 1. The amount of difference between these two profiles is evenly included in the model at every time step during the phase II. Note that the compensating effect of the Coriolis drifting is excluded in the calculation of the modified basic-state wind profile. The modified basic-state wind profile shows a strong positive wind shear ($7.6 \times 10^{-3} \text{ s}^{-1}$) in the lower layer (below 2.5 km), a weak positive shear ($1.1 \times 10^{-3} \text{ s}^{-1}$) in the middle layer ($2.5 \text{ km} < z < 5.5 \text{ km}$), a moderate negative wind shear ($-4.6 \times 10^{-3} \text{ s}^{-1}$) in the mid-to-upper layer ($5.5 \text{ km} < z < 9 \text{ km}$), and a weak positive shear ($2.5 \times 10^{-3} \text{ s}^{-1}$) in the upper troposphere ($9 \text{ km} < z < 14 \text{ km}$).

The change in the basic-state wind by the cloud momentum flux of on the order of $10 \text{ m s}^{-1}/\text{hr}$ is quite significant. This suggests that the basic-state wind in which organized mesoscale convective system is imbedded needs to be considered time-dependent rather than to be constant with time. In other words, interaction between the large-scale environment and mesoscale convective system should be considered within a time scale of several hours. In most of the numerical modeling

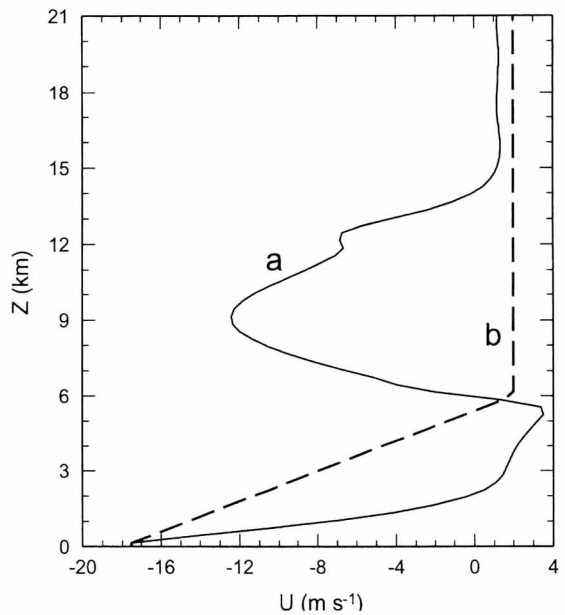


Fig. 8. The modified basic-state wind profile (curve a) and the initial basic-state wind profile (curve b).

studies of mesoscale convective storms, interaction between the large-scale basic-state flow and mesoscale convective system has not been considered in a proper way. That is, only one-way interaction from the large-scale flow to mesoscale convective storms using different time-independent basic-state flows has been taken into account. In this study, we attempt to include an interaction between the large-scale flow and organized mesoscale convective storm in one of plausible ways and investigate how both the basic-state flow and mesoscale convective storm can be affected by the interaction. This constitutes an essence of the present study.

Figure 9 shows the time series of the domain maximum vertical velocity in the variable simulation. Before $t = 6$ h, the result of the variable simulation is identical to that of the control simulation because the basic-state wind is the same in the two cases. During the period of $t = 6-8$ h, the basic-state wind smoothly changes from the initial profile to the modified one shown in Fig. 8 and the time series of the maximum vertical velocity deviates from that in the control simulation. After $t = 8$ h, the periodic oscillation of the maximum vertical velocity shown in the control simulation disappears and oscillation with very short

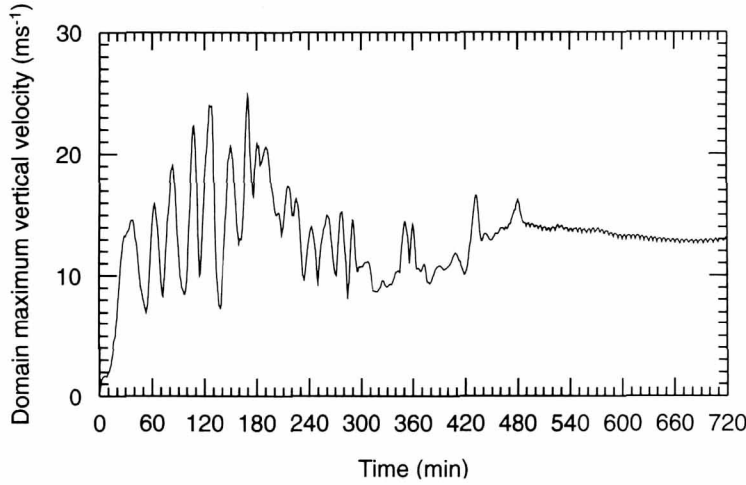


Fig. 9. The time series of the domain maximum vertical velocity in the variable simulation.

period (about 5 min) and negligible amplitude is observed. This high frequency oscillation is not related to the periodic regeneration of convective cell behind GFU. Rather, it is more likely the trivial impact of acoustic waves which are below the cutoff (Brunt-Vaisala frequency) for gravity waves.

The evolution of the surface precipitation rate (Fig. 10) shows that the precipitation is concentrated in the GFU region after $t = 8$ h and that unlike the control simulation no major periodic cells behind the GFU are observed. Also, after $t = 8$ h, the gust front propagates upstream with a speed of 3.3 m s^{-1} relative to the gust front in the control simulation. The speed of the gust front in the variable simulation is faster than that in the control simulation because of the increased basic-state wind shear in the lower layer. Figure 10 indicates that there exists the regime transition at 8 h from the typical multicell-type behavior to singlecell-type one. The singlecell-type convective storm is almost steady throughout the simulation after 8 h. To some extent, this singelcell-type storm is similar to the unicellular storm by Dudhia *et al.* (1987). They characterized the unicellular storm by almost steady, vertical updraft, weak downdraft, and no density current, which can be considered as a solitary waves. In the present study, two different types of convective storms can be produced during the evolution of the convective system by changing the basic-state wind with time, while they

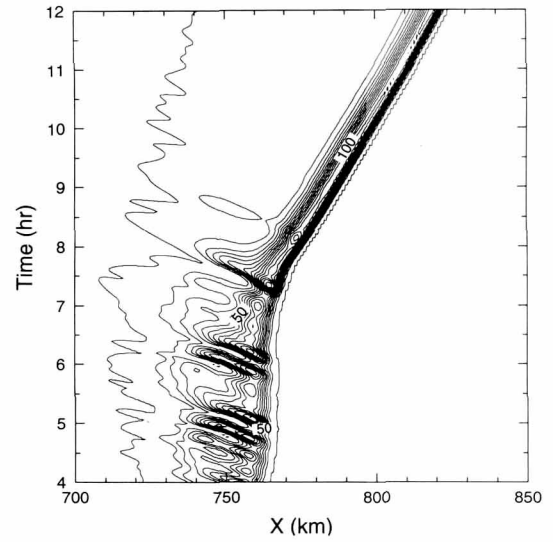


Fig. 10. The evolution of the surface precipitation rate after $t = 4$ h in the variable simulation. The contour interval is 10 mm hr^{-1} except that the contours in the left and right boundaries are 0.1 mm hr^{-1} .

were produced by two different initial basic-state wind profiles in Dudhia *et al.* (1987).

Differences between the control and variable simulations are clearly seen from the vertical velocity field superimposed on the equivalent potential temperature field at $t = 10$ h (Fig. 11). In the variable simulation, there exists an almost erect updraft at the gust front

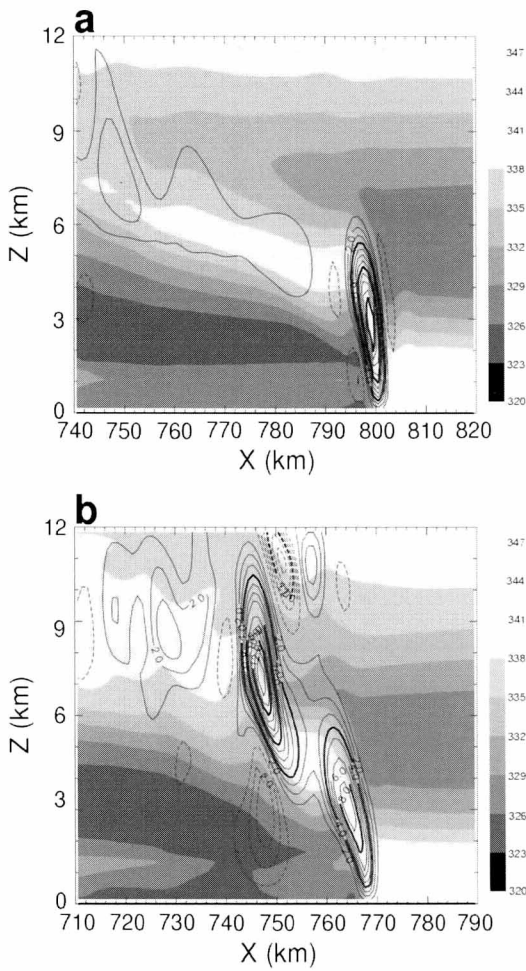


Fig. 11. The vertical velocity field superimposed on the equivalent potential temperature field at $t = 10$ h in (a) the variable simulation and (b) the control simulation.

that is vertically extended up to $z = 6$ km and no major convective cells behind the updraft are observed. This situation is similar to that explained by Fovell and Tan (1998) (see Fig. 10d in their paper) in which the positively buoyant convective cell is at the top of the GFU and the GFU becomes strongest and tallest. Based on the Fovell and Tan's result, this is just one of stages in the periodic cycle of multicell storms. However, in the present variable simulation, this situation is almost steady as will be shown in Fig. 12 and the convective cell at the top of the GFU cannot be separated from the GFU. Downdraft in the lower layer near $x = 798$ km is very weak and localized

just beneath the almost erect GFU compared with that (near $x = 750$ km) behind the GFU in the control simulation (Fig. 11b). The perturbation equivalent potential temperature field (not shown) indicates that evaporative cooling takes place in a very localized region (within the downdraft cell) for the case of variable simulation, while it is widely spread behind the major convective cell for the case of control simulation. This is dynamically similar to the unicell-type convective storm in Dudhia *et al.* (1987). The weak updraft extended rearward and tilted upshear in the region of $x < 788$ km seems to be internal gravity waves induced by the steady GFU. The strength of the gravity waves changes slightly with time in a 5 min period as that of the GFU. In contrast, in the control simulation, there exists a GFU near $x = 768$ km. A major convective cell behind the GFU is centered at $x = 747$ km, which is already at the decaying stage. A new convective cell is developing in between the GFU and the major convective cell. The weak updrafts behind the major convective cell are propagating convective cells that had already an experience of being a major convective cell in the previous oscillation periods. In the variable simulation, the highest equivalent potential temperature in the planetary boundary layer ahead of the gust front cannot reach rearward following the front-to-rear inflow (Fig. 11a), while it reaches far enough to feed the new cell in the control simulation (Fig. 11b).

Figure 12 shows the evolution of the vertical velocity field superimposed on the perturbation potential temperature in every 5 min from $t = 10$ h to $t = 10$ h 35 min. The GFU is almost steady in the shape and intensity, which propagates upstream with a speed of 3.3 m s^{-1} relative to the gust front in the control simulation. The updraft cells behind the GFU are very weak compared with those in the control simulation and their behavior is not the same as that in typical multicell-type convective storms. Even though there exists a minor indication of separation, amplification, and decay processes of convective cells behind the GFU, they are diminished after $t = 10$ h 30 min.

The steadiness of GFU is distinctive feature compared with periodic characteristics of multicell-type convective storm by control simulation. Similar results were obtained for the unicell squall line case by Dudhia *et al.* (1987). They suggested that the behavior of steady

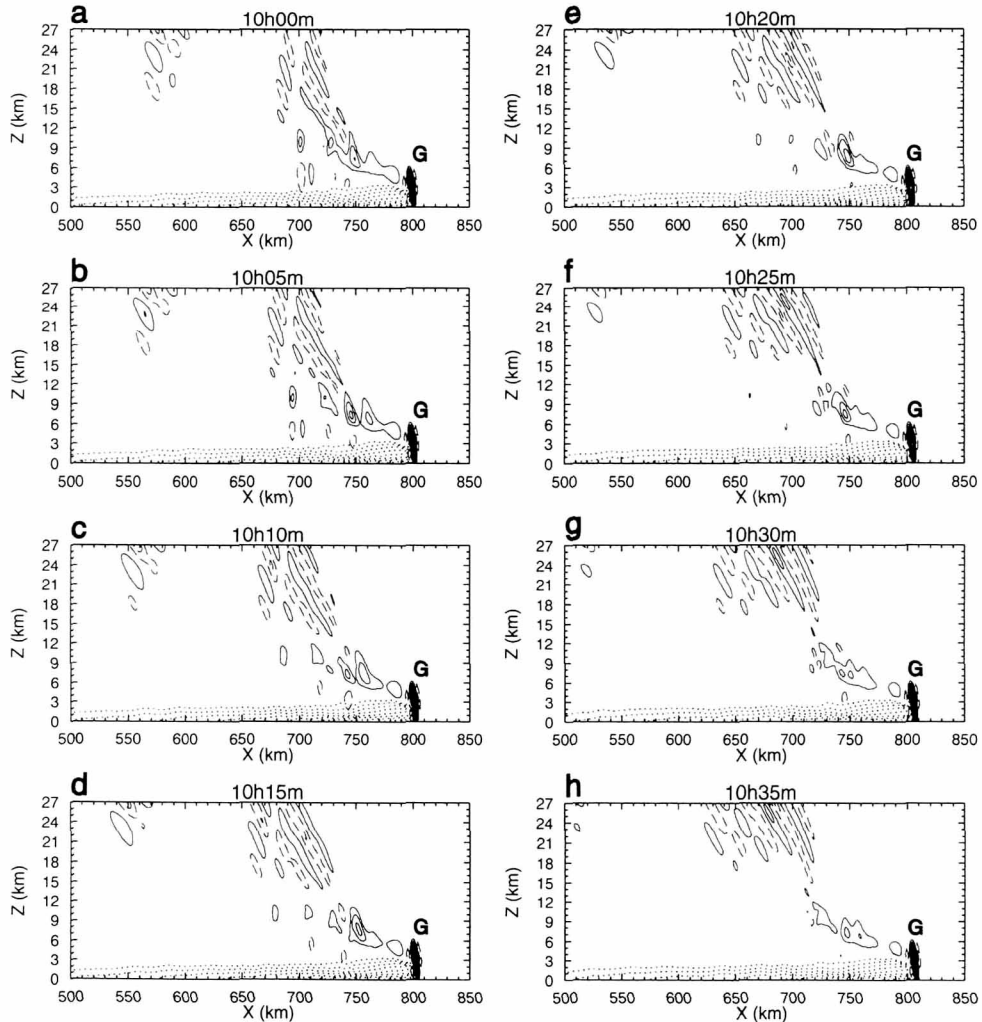


Fig. 12. The evolution of the vertical velocity field superimposed on the perturbation potential temperature field in every 5 min from $t = 10$ h to $t = 10$ h 35 min in the variable simulation. Only the negative perturbation potential temperature is plotted to clearly represent the cold outflow. The contour intervals of the vertical velocity and perturbation potential temperature are 1 m s^{-1} and 1 K , respectively.

unicellular convection dynamically resembles stationary convection over an isolated ridge. That is, the steady updraft is likely to be a solitary wave of elevation. Because the updraft is almost vertical in unicell case, the rain falls in the lower part of updraft branch so that ascending air near the ground with highest equivalent potential temperature will be returned back to the ground behind the GFU. The evaporatively cooled, water-laden downdraft in the lower layer produces localized, weak

high pressure region converged with boundary layer air in the downdraft branch, which can lift an air parcel effectively to the level of free convection. This flow pattern also resembles a stationary cold pool case by Lin and Chun (1991), which produced a steady updraft at the head of relatively weak cold pool against the inflow. In Fig. 12, density current represented by the negative temperature perturbation is shown to be well developed even though the magnitude is much smaller

than that by the control simulation (Fig. 4), contrast to the results by Dudhia *et al.* (1987) and Lin and Chun (1991). This is because the density current was developed in the previous time (before 8 h) when the convection was in the multicell regime.

One of interesting features in Fig. 12 is that convectively generated gravity waves above clouds are induced mainly by the convective cells behind the GFU rather than the GFU. Because a critical level is located near $z = 6$ km against the gust front, gravity waves generated by the almost steady GFU may not propagate upward. On the other hand, the convective cells behind the GFU produce vertically propagating gravity waves. The convective cells behind the GFU do not feel the critical level located near $z = 6$ km because they propagate rearward relative to the GFU. Actually, the critical level for individual convective cell behind the GFU is closer to the surface as the cell propagates slower relative to the GFU (located in the rearward side in a snapshot). Thus, the basic-state wind relative to each convective cell in the cloud region and above blows from the left to right. This is clearly seen from the westward phase tilt of gravity waves above clouds in order for wave energy to propagate upward.

Figures 9–12 show that consecutive cells behind the GFU do not appear in the variable simulation because the convective cell at the top of the GFU cannot be separated from the GFU. One of possible reasons for preventing the cut-off process is related to the storm-relative inflow that changes with time in the variable simulation. In the present study, the change in the basic-state wind is represented in the model through the change in the total wind or storm-relative inflow far upstream.

Figure 13 shows the storm-relative inflow at 5 km ahead of the GFU at selected four times of the variable simulation and one time (last of the four times) of the control simulation. It is clearly seen that the magnitude of the storm-relative inflow near the GFU decreases rapidly with time and the storm-relative inflow reverses its sign above $z = 6$ km. The difference between the storm-relative inflows in the control and variable simulations is largest at the last time ($t = 8$ h 20 min).

Recently, Lin *et al.* (1998) showed that the periodicity of multicell storms is strongly related to the magnitude

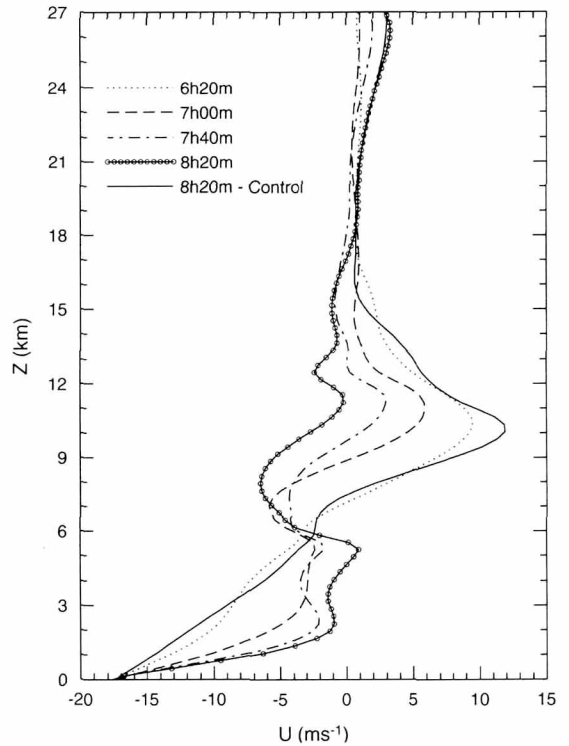


Fig. 13. The storm-relative inflow at 5 km ahead of the gust front at selected four times of the variable simulation and one time (last of the four times) of the control simulation.

of the storm-relative mid-level inflow. They suggested that the convective cell is separated from GFU through the advection by the storm-relative mid-level inflow. It was shown that the period of cell regeneration is inversely proportional to the magnitude of the storm-relative mid-level inflow. Figure 14 shows the time series of the storm-relative mid-level inflow, vertically averaged from $z = 3$ km to 6 km, at 5 km ahead of the GFU at each time in the variable and control simulations. In the variable simulation, the magnitude of the storm-relative mid-level inflow decreases rapidly with time and it is close to zero after $t = 8$ h. In contrast, in the control simulation, the storm-relative mid-level inflow is quasi-steady with values of about $6\text{--}7 \text{ m s}^{-1}$. It appears that the very weak storm-relative mid-level inflow prevents a separation of convective cell from the GFU. That is, the period of convective cell regeneration might be infinite for the near-zero storm-relative mid-level inflow, hence a new cell will never appear behind the GFU.

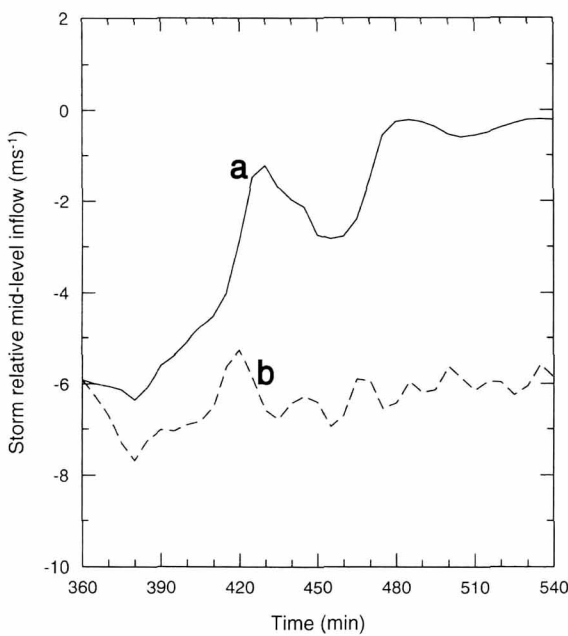


Fig. 14. The time series of the storm-relative mid-level inflow, vertically averaged from $z = 3$ km to 6 km, at 5 km ahead of the gust front updraft at each time in the variable simulation (curve a) and the control simulation (curve b).

5. Summary and conclusions

Effects of time-varying basic-state wind representing the large-scale flow on multicell-type convective storms were investigated numerically using a two-dimensional cloud model (ARPS). Two types of numerical experiments were performed, the control simulation with time-independent basic-state wind and the variable simulation with time-dependent basic-state wind. The change in the basic-state wind in the variable simulation was obtained by the vertical convergence of the cloud momentum flux in the troposphere and the cloud-generated gravity-wave momentum flux in the stratosphere.

It was shown that the cloud momentum flux produces positive basic-state wind shear in the lower and upper troposphere and negative shear in the mid-troposphere. The amount of wind change by the momentum flux was significant ($\sim 10 \text{ m s}^{-1}/\text{hr}$). This resulted in a significant structural change of the mesoscale convective system. The typical multicell-type characteristics of convective storms, such as periodic convective cell

generation, development, and decay behind the gust front updraft, produced in the control simulation disappeared in the variable simulation, and convection was concentrated in the gust front updraft region. That is, the periodic regeneration of convective cell behind the gust front updraft was no longer possible in the variable simulation. It was found that very weak storm-relative mid-level inflow in the variable simulation prevents a separation of convective cell from the gust front updraft, which is essential for the cell regeneration in multicell-type storms.

This study is based on the concept that timely or/and horizontally averaged model-produced total wind cannot be the large-scale environmental flow in a two-dimensional, non-rotating framework. The environmental flow can be the slow-manifold, rotationally-constrained flow. The mesoscale convective system in a two-dimensional, non-rotating framework only can modify the environmental flow largely due to the change in the potential vorticity field brought about by convective mass transport, latent heating/cooling, and mixing. The influence of mesoscale convective system on the large-scale flow can be estimated by calculating the flux divergences of heat, momentum, and moisture, even though a portion of energy is used for gravity waves. Therefore, feedback between the large-scale basic-state flow and mesoscale perturbations cannot be automatically considered by simply running a nonlinear mesoscale numerical model. In order to take into account an interaction between the large-scale environment and mesoscale convective storms for mesoscale numerical modeling, extra treatment, such as what we proposed in this study, is needed. Because the timely or/and horizontally averaged model-produced total wind (mean wind) is not the large-scale flow (basic-state wind), there is no double-counting of the convective momentum flux.

The results of the present study suggests that the time variation of the basic-state wind should be considered in the study of mesoscale convective storms even with a time scale of several hours. Once convective storm generates updrafts on the order of 20 m s^{-1} or larger, the large-scale flow can be changed significantly and the previous structure of the convective storm will be no longer maintained. Especially, multicell-type convective storms known to produce convective cells

periodically under time-independent basic-state wind may not be so realistic even in a numerical modeling point of view. In other words, interaction between the large-scale flow and organized mesoscale convective storms should be considered. In the present study, we attempted to examine an interaction between the large-scale flow and mesoscale convective storms in a mesoscale point of view using one of plausible ways. Because the change in the basic-state flow considered here comes from the mesoscale convective system itself, interaction between the mesoscale convective system and large-scale flow was treated with some limitations.

Several questions remain to be answered. First, what is a proper way to interact the large-scale flow and mesoscale convective storms? This is an important issue both in mesoscale and large-scale numerical modeling studies. Recent attempts to include the effects of organized mesoscale convective storms through the momentum and heat fluxes in currently used cumulus parameterization schemes (e.g., Moncrieff 1992; Wu and Moncrieff 1996) may be one way. Parameterizing the effects of gravity-wave drag induced by convective clouds in large-scale models (e.g., Kershaw 1995; Chun and Baik 1998) may be other way of including such an interaction in large-scale models. Thus far, there have been no proper mesoscale modeling studies considering two-way interaction between the large-scale flow and mesoscale convective storms even with a limited way. The present study might provide a first step for considering such an interaction in modeling mesoscale convective storms. When the interaction is included in a numerical model, a time-lag between the convective activity and its impact on the large-scale flow should be determined in advance. This might be equally important in large-scale models to parameterize the effects of mesoscale convective system. Even though a 2 h lag was used in the present study, there is no theoretical basis for that. Sensitive tests of the interaction period and methodology deserve a further study.

Secondly, in the present study, the effects of change in basic-state thermodynamic variables by cloud heat and moisture fluxes were not considered. There is no justification for neglecting these effects. Furthermore, because the large-scale flow is approximately in a thermal wind balance, change in the basic-state wind implicitly requires change in the temperature field. Note

that change in the meridional temperature gradient by the vertical shear of the horizontal wind is not included in the present two-dimensional modeling study. Change in the large-scale temperature and water vapour mixing ratio can be calculated using temporal and spatial average of simulated heat and moisture fluxes.

Thirdly, the change in the basic-state wind was calculated only by the vertical convergence of the momentum flux as a subgrid-scale momentum forcing. However, for the large-scale flow, the Coriolis drift of the secondary circulation induced by the subgrid-scale momentum forcing can significantly compensate for the basic-state wind acceleration/deceleration. In the present case, the basic-state wind acceleration by the Coriolis force through the secondary circulation (not shown) compensates for the basic-state wind acceleration by the momentum forcing by about 32% in the lower troposphere and about 20% in the mid-to-upper troposphere according to a linear calculation. If this compensation was included in the calculation of the basic-state wind change, resultant storm structure in the variable simulation would be changed. Also, a nonlinear form of turbulent diffusion by subgrid-scale motion will affect basic-state wind change, even though its magnitude is not so large in the present case.

Acknowledgment. The authors are very grateful to Dr. Glenn Shutts of the UKMO for fruitful discussion on the conceptual validity of the methodology introduced in this paper and to Dr. Mitchell Moncrieff of the NCAR for valuable comments on transition between the multicell storms and single cell storm. The authors are also grateful to Dr. R. B. Nance for discussion on the smooth transition technique for time-varying basic-state wind. The authors wish to acknowledge the financial support of the Korea Research Foundation made in the program year of 1998 and the Brain Korea 21 Program. Numerical computations were carried out on the Cray C90 at the KORDIC.

REFERENCES

- Chun H.-Y., and J.-J. Baik, 1998: Momentum flux by thermally induced internal gravity waves and its approximation for

- large-scale models. *J. Atmos. Sci.*, **55**, 3299-3310.
- Dudhia, J., and M. W. Moncrieff, 1987: A numerical simulation of quasi-stationary tropical convective bands. *Q. J. R. Meteorol. Soc.*, **113**, 929-967.
- _____, M. W. Moncrieff, and D. W. K. So, 1987: The two-dimensional dynamics of West African squall lines. *Q. J. R. Meteorol. Soc.*, **113**, 121-146.
- Fovell, R. G., D. R. Durran, and J. R. Holton, 1992: Numerical simulation of convectively generated stratospheric gravity waves. *J. Atmos. Sci.*, **49**, 1427-1442.
- _____, and P. S. Dailey, 1995: The temporal behavior of numerically simulated multicell-type storms. Part I: Mode of behavior. *J. Atmos. Sci.*, **52**, 2073-2095.
- _____, and P.-H. Tan, 1998: The temporal behavior of numerically simulated multicell-type storms. Part II: The convective cell life cycle and cell regeneration. *Mon. Wea. Rev.*, **126**, 551-577.
- Hauf, T., and T. L. Clark, 1989: Three-dimensional numerical experiments on convectively forced internal gravity waves. *Q. J. R. Meteorol. Soc.*, **115**, 309-333.
- Kershaw, R., 1995: Parameterization of momentum transport by convectively generated gravity waves. *Q. J. R. Meteorol. Soc.*, **121**, 1023-1040.
- Klemp, J. B., and R. B. Wilhelmson, 1978: The simulation of three-dimensional convective storm dynamics. *J. Atmos. Sci.*, **35**, 1070-1096.
- Krueger, S. K., 1988: Numerical simulation of tropical cumulus clouds and their interaction with the subcloud layer. *J. Atmos. Sci.*, **45**, 2221-2250.
- Lafore, J.-P., and M. W. Moncrieff, 1989: A numerical investigation of the organization and interaction of the convective and stratiform region of tropical squall lines. *J. Atmos. Sci.*, **46**, 521-544.
- LeMone, M. A., 1983: Momentum transport by a line of cumulonimbus. *J. Atmos. Sci.*, **40**, 1815-1834.
- Lin, Y.-L., and H.-Y. Chun, 1991: Effects of diabatic cooling in a shear flow with a critical level. *J. Atmos. Sci.*, **48**, 2476-2491.
- _____, R. L. Deal, and M. S. Kluie, 1998: Mechanisms of cell regeneration, development, and propagation within a two-dimensional multicell storm. *J. Atmos. Sci.*, **55**, 1867-1886.
- Moncrieff, M. L., 1992: Organized convective system: Archetypal dynamical models, mass and momentum flux theory, and parameterization. *Q. J. R. Meteorol. Soc.*, **118**, 819-850.
- _____, and J. S. A. Green, 1972: The propagation and transfer properties of steady convective overturning in shear. *Q. J. R. Meteorol. Soc.*, **98**, 336-352.
- Nance, L. B., and D. R. Durran, 1997: A modeling study of nonstationary trapped mountain lee waves. Part I: Mean-flow variability. *J. Atmos. Sci.*, **54**, 2275-2291.
- Newton, C. W., 1950: Structure and mechanism of the prefrontal squall line. *J. Meteor.*, **7**, 210-222.
- _____, and H. R. Newton, 1959: Dynamical interaction between large convective clouds and environment with vertical shear. *J. Meteor.*, **16**, 483-496.
- Ogura, Y., and M. T. Liou, 1980: The structure of a midlatitude squall line: A case study. *J. Atmos. Sci.*, **37**, 553-567.
- Orlanski, I., 1976: A simple boundary condition for unbounded hyperbolic flows. *J. Comput. Phys.*, **21**, 251-269.
- Palmer, T. N., G. J. Shutts, and R. Swinbank, 1986: Alleviation of a systematic westerly bias in general circulation and numerical weather prediction models through an orographic gravity wave drag parameterization. *Q. J. R. Meteorol. Soc.*, **112**, 1001-1039.
- Rotunno, R., J. B. Klemp, and M. L. Weisman, 1988: A theory for strong, long-lived squall lines. *J. Atmos. Sci.*, **45**, 463-485.
- Smagorinsky, J., 1963: General circulation experiments with the primitive equations. I. The basic experiment. *Mon. Wea. Rev.*, **91**, 99-164.
- Soong, S.-T., and W.-K. Tao, 1980: Response of deep tropical cumulus clouds to mesoscale processes. *J. Atmos. Sci.*, **37**, 2016-2034.
- Tao, W.-K., J. Simpson, and S.-T. Soong, 1987: Statistical properties of a cloud ensemble: A numerical study. *J. Atmos. Sci.*, **44**, 3175-3187.
- Thorpe, A. J., M. J. Miller, and M. W. Moncrieff, 1980: Dynamical models of two-dimensional downdraughts. *Q. J. R. Meteorol. Soc.*, **106**, 463-484.
- _____, M. J. Miller, and M. W. Moncrieff, 1982: Two-dimensional convection in non-constant shear: A model of mid-latitude squall lines. *Q. J. R. Meteorol. Soc.*, **108**, 739-762.
- Weisman, M. L., and J. B. Klemp, 1982: The dependence of numerically simulated convective storms on wind shear and buoyancy. *Mon. Wea. Rev.*, **110**, 504-529.
- _____, J. B. Klemp, and R. Rotunno, 1988: The structure and evolution of numerically simulated squall lines. *J. Atmos. Sci.*, **45**, 1990-2013.
- Wu, X., and M. W. Moncrieff, 1996: Collective effects of organized convection and their approximation in general circulation models. *J. Atmos. Sci.*, **53**, 1477-1494.
- Xue, M., K. K. Droegemeier, V. Wong, A. Shapiro, and K. Brewster, 1995: *ARPS version 4.0 User's Guide*. Center for Analysis and Prediction of Storms, University of Oklahoma, 380pp.
- Yang, M.-J., and R. A. Houze Jr., 1995: Multicell squall line structure as a manifestation of vertically trapped gravity waves. *Mon. Wea. Rev.*, **123**, 641-660.

구름 운동량 속에 의해 시간적으로 변하는 기본류가 다중 세포형 뇌우에 미치는 영향

전혜영¹ · 송인선¹ · 백종진²

¹연세대학교 대기과학과, 지구환경연구소 · ²서울대학교 지구환경과학부

(2001년 12월 1일 접수; 2001년 12월 20일 채택)

요약

다중세포형 중규모 대류계에 미치는 구름 운동량속에 의해 시간적으로 변화하는 기본류의 영향을 2차원 구름 수치모형을 이용하여 고찰하였다. 기본류를 시간적으로 변화시키지 않은 규준 실험과 기본류가 시간적으로 변화하도록 한 variable 실험을 수행하였다. 기본류의 변화량은 구름에 의한 운동량속의 연직 수렴함을 계산하여 추정하였다. 구름 운동량속에 의한 기본류의 변화는 최대 $10 \text{ m s}^{-1}/\text{hr}$ 였으며, 구름 운동량속은 대류권 하부의 양의 시어를 증가시켰으며 대류권 중부와 상부에 각각 음과 양의 연직 시어를 유도하였다. 이와 같은 기본류의 변화는 중규모 대류계를 상당히 변화시켰다. 즉, 규준 실험에서 나타났던 대류는 돌풍전선 앞에서 새로운 대류세포가 주기적으로 생성되어 돌풍전선의 후면으로 전파되는 다중세포형 대류계였으나 variable 실험에서는 대류가 돌풍전선 앞에 집중되었으며 새로운 대류세포의 발생이 일어나지 않았다. 이는 대류계의 전단에서 불어오는 중간 대류권의 바람이 매우 약하여 돌풍전선으로부터 대류세포를 분리시킬 수 없음에 기인한 것이다.

Key words: 다중세포형 대류계, 기본류, 구름 운동량속